Dynamic Response of Two-Layered Cylindrical Shells to Time-Dependent Loads

DAVID BUSHNELL*
Lockheed Missiles and Space Company, Palo Alto, Calif.

A modal analysis is used to predict the response to time-dependent loads of a finite-length, simply supported elastic circular cylindrical shell composed of two bonded isotropic layers. A shell of infinite length subjected to an external load with no axial component is also analyzed. Calculations were made for the specific case of a two-layered cylindrical shell loaded impulsively by a lateral blast distributed sinusoidally around half of the circumference. It is found that, for the particular loading treated, the axial stress in the finite-length shell has a larger amplitude than the circumferential stress, even though the load has no axial component and even though the shell is not axially constrained in any way at the edges. A dynamic edge effect is seen to propagate into the shell. Use of a "ring" model of an infinite-length shell subjected to an axially uniform pressure pulse leads to an accurate prediction of the normal stresses at the middle of the finite shell for very early response times. However, the radial displacement response is four times as great for the "ring" as for the finite shell, and the fundamental frequency of the "ring" is a seventh of that for the finite shell. The axial stress amplitude predicted by the "ring" model ($\sigma_x = \nu\sigma_\theta$) is much smaller than that predicted by the finite-length model, and of course no edge effect is possible in the "ring."

Nomenclature

x	=	axial coordinate
θ	=	circumferential coordinate
z	=	radial coordinate, positive inward
u^*, v^*, w^*	=	axial, circumferential, radial displacements
u, v, w	=	$u^*/a, v^*/a, w^*/a$
a, h, L	=	radius, thickness, length of shell
k	=	$h^2/12a^2$
ρ	=	mass density of shell wall material
E	=	Young's modulus
ν	=	Poisson's ratio
p_i	=	$i = 1, 2, 3$ axial, circumferential, radial pressure
q_i	=	$p_i\, a(1 - \nu^2)/Eh$
$(\ )'$	=	$a\partial(\ )/\partial x$
$(\ )\cdot$	=	$\partial(\ )/\partial\theta$
ω_0	=	$\{E/[\rho a^2(1 - \nu^2)]\}^{1/2}$
τ	=	$\omega_0 t$
E_1, E_2	=	Young's moduli of inner, outer layers (Fig. 2)
d_1, d_2	=	thicknesses of inner, outer layers
ν_1, ν_2	=	Poisson's ratios of inner, outer layers
ρ_1, ρ_2	=	densities of inner, outer layers
$\omega_0{}^*$	=	$[(E_1d_1 + E_2d_2)/(\rho_1d_1 + \rho_2d_2)a^2(1 - \nu^2)]^{1/2}$
$q_i{}^*$	=	$p_i\, a(1 - \nu^2)/(E_1d_1 + E_2d_2)$
t_0	=	duration of impulse, sec
$\tau_0{}^*$	=	$\omega_0{}^* t_0$
σ^*	=	dimensionless stress, $\sigma^* = \sigma\pi(1 - \nu^2)/E_1q_0{}^*\tau_0{}^*$
Ω	=	ω/ω_0 or $\omega/\omega_0{}^*$
i_j	=	unit vector in jth direction
$\Psi_{mn}{}^i$	=	(i, m, n)th free vibration vector mode
$\eta_{mn}{}^i$	=	(i, m, n)th generalized coordinate
$M_{mn}{}^i$	=	(i, m, n)th dimensionless generalized mass
$\Omega_{mn}{}^i$	=	(i, m, n)th angular frequency parameter

1. Introduction

MANY papers have been written on the free vibration characteristics of thin cylindrical shells with various edge conditions. Lord Rayleigh found the natural frequencies of a cylindrical shell with free edges in 1894.[1] In 1948 Arnold and Warburton[2] investigated the free vibrations of a simply supported cylinder whose ends were constrained to remain circular. Baron and Bleich[3] in 1954 used an energy approach to construct a table of natural frequencies and mode shapes for infinitely long cylindrical shells, and in the same year Yu[4] studied finite-length cylindrical shells with simply supported and clamped edges. In 1958, Yu[5] included rotatory inertial and transverse shear effects in his analysis. More recently, Forsberg[6] presented a thorough analysis of the effect of boundary conditions on the natural frequencies of cylindrical shells.

Humphreys and Winter[7] calculated the stresses in an infinitely long cylindrical shell subjected to a time-dependent lateral blast distributed sinusoidally over half of the circumference and uniformly along the axis. They used a Laplace transform approach. Their results showed that the response is independent of the pulse shape for pulse times less than $0.1\ a/c$, where a is the radius of the shell and c is the speed of sound in the wall material, and that bending effects are small, especially for early times in the response.

Sheng[8] applied the modal approach and Williams' method to find the response of thin, finite-length cylindrical shells to transient surface loading. He used the free-vibration characteristics of a simply supported cylinder to compute the displacements and the stresses resulting from an arbitrary dynamic load distribution on the surface. The generalized coordinates corresponding to the forcing function were obtained, and the displacements and stresses were expanded in infinite series, the coefficients of whose terms correspond to the free-vibration modes.

Here, similar methods are used to determine the response of a finite-length cylindrical shell of two bonded isotropic layers to time-dependent loads. The particular cases of finite-length and infinite-length shells subjected to a nonsymmetric radial blast load are studied. Since the basic theory has been thoroughly presented in Sheng's paper,[8] it will be briefly outlined only. More detailed attention will be given to the numerical results.

2. Formulation and Solution of the Problem

The problem of a simply supported, finite-length cylindrical shell loaded in an arbitrary manner will be considered first. No rigid body motions will be included in the analysis.

Received January 4, 1965; revision received May 17, 1965. The work presented here is part of a dissertation submitted to Stanford University in partial fulfillment of the requirements for the Ph.D. degree. Professor N. J. Hoff, Head, Department of Aeronautics and Astronautics, served as advisor. The research for this report was completed at Lockheed Missiles and Space Company in cooperation with the Bureau of Naval Weapons under Contract No. NOw 63-0050-C.

* Research Specialist.

The differential equations governing the motion of such a shell in the axial, circumferential, and radial directions were formulated by Flügge[9] in 1934; in dimensionless form they are, respectively,

$$L_1(u, v, w) - u_{\tau\tau} = -q_1 \tag{2.1}$$

$$L_2(u, v, w) - v_{\tau\tau} = -q_2 \tag{2.2}$$

$$L_3(u, v, w) - w_{\tau\tau} = -q_3 \tag{2.3}$$

where the L_i are the space differential operators derived by Flügge (Ref. 9, p. 219). Subscript τ denotes differentiation with respect to the dimensionless time parameter τ defined by

$$\tau \equiv \omega_0 t \tag{2.4}$$

where ω_0 is the fundamental extensional angular frequency, that is, the frequency of the mode in which the entire shell performs uniform radial motion. The radial pressure parameter q_3 and the radial displacement w are positive inward. Figure 1 shows the sign convention used. The simple-support boundary conditions are

$$v = w = M_x = N_x = 0 \text{ at } x = 0 \text{ and } L \tag{2.5}$$

The boundary-value problem presented in Eqs. (2.1–2.3 and 2.5) can be solved by expanding the displacement vector

$$\bar{d} \equiv \bar{\imath}_1 u + \bar{\imath}_2 v + \bar{\imath}_3 w = \begin{Bmatrix} u \\ v \\ w \end{Bmatrix} \tag{2.6}$$

in an infinite series of free vibration mode displacements:

$$\bar{d} = \sum_{m=1}^{\infty} \sum_{n=0}^{\infty} \sum_{i=1}^{3} \bar{\psi}_{mn^i}(x, \theta)\eta_{mn^i}(\tau) \tag{2.7}$$

The vector modes $\bar{\psi}_{mn^i}$ defined by

$$\begin{Bmatrix} u_{mn^i} \\ v_{mn^i} \\ w_{mn^i} \end{Bmatrix} \equiv \bar{\psi}_{mn^i} = \begin{Bmatrix} (A/C)_{mn^i} \cos(m\pi x/L) \cos n\theta \\ (B/C)_{mn^i} \sin(m\pi x/L) \sin n\theta \\ \sin(m\pi x/L) \cos n\theta \end{Bmatrix} \tag{2.8}$$

correspond to displacements symmetric only with respect to θ. Any loading $\bar{q}$ can be expressed as a sum of symmetric and antisymmetric components. The orthogonality of the eigenvectors $\bar{\psi}_{mn^i}$[8] assures that the symmetric component of the load excites only symmetric displacement modes, and the antisymmetric component excites only antisymmetric modes. Henceforth, only the symmetric part of the boundary-value problem is considered explicitly. The antisymmetric part can be developed in the same way except that wherever $(B/C)_{mn^i}$, $\sin n\theta$, and $\cos n\theta$ occur in the analysis of the symmetric part, they are replaced by $-(B/C)_{mn^i}$, $\cos n\theta$, and $\sin n\theta$, respectively.

The generalized coordinates $\eta_{mn^i}(\tau)$ are calculated from the equation

$$(\eta_{mn^i})_{\tau\tau} + (\Omega_{mn^i})^2\eta_{mn^i} = \frac{1}{M_{mn^i}} \int_0^L \int_0^{2\pi} \bar{q} \cdot \bar{\psi}_{mn^i} a d\theta dx \tag{2.9}$$

The angular frequency parameters Ω_{mn^i} are the eigenvalues of the free-vibration problem [homogeneous equivalent of Eqs. (2.1–2.3) with Eq. (2.5)], and the summation from one to three on the index i in Eq. (2.7) is necessary to account for the three eigenvalues Ω_{mn^i} and eigenvectors $\bar{\psi}_{mn^i}$ that exist for each given set (m, n), when $n \neq 0$. When $n = 0$, there are only two eigenvalues corresponding to the symmetric modes for each value of m. Ascending values of the superscript i correspond to ascending frequencies. The displacement ratios $(A/C)_{mn^i}$ and $(B/C)_{mn^i}$ are uniquely determined from the free-vibration problem once the eigenvalues Ω_{mn^i} are known. The quantity M_{mn^i} is the generalized mass, given by

$$M_{mn^i} = \int_0^L \int_0^{2\pi} \bar{\psi}_{mn^i} \cdot \bar{\psi}_{mn^i} a d\theta dx \tag{2.10}$$

and the stresses in the shell can be computed from Hooke's law, using the strain-displacement relations given by Flügge (Ref. 9, p. 212). Expressed in terms of the free-vibration mode displacements, they are

$$\sigma_\theta = \frac{E}{1 - \nu^2} \sum_{m=1}^{\infty} \sum_{n=0}^{\infty} \sum_{i=1}^{3} D_{mn^i} \sin\frac{m\pi x}{L} \cos n\theta \eta_{mn^i}(\tau) \tag{2.11}$$

$$\sigma_x = \frac{E}{1 - \nu^2} \sum_{m=1}^{\infty} \sum_{n=0}^{\infty} \sum_{i=1}^{3} E_{mn^i} \sin\frac{m\pi x}{L} \cos n\theta \eta_{mn^i}(\tau) \tag{2.12}$$

$$\tau_{x\theta} = \frac{E}{2(1 + \nu)} \sum_{m=1}^{\infty} \sum_{n=0}^{\infty} \sum_{i=1}^{3} F_{mn^i} \cos\frac{m\pi x}{L} \sin n\theta \eta_{mn^i}(\tau) \tag{2.13}$$

where D_{mn^i}, E_{mn^i}, and F_{mn^i} are known functions of $(A/C)_{mn^i}$, $(B/C)_{mn^i}$, ν, m, n, L/a, and z/a.

Cylindrical Shell of Infinite Length

If the length-to-radius ratio is allowed to approach infinity, $q_1 = 0$, and q_2 and q_3 are independent of x, and the problem approaches that of a shell deforming in plane strain. Such a shell can be idealized as a ring loaded only in its plane. The boundary-value problem defined by Eqs. (2.1–2.3) can be solved as before by considering separately symmetric and antisymmetric loads and displacements. Only the symmetric components will be considered in the following discussion.

The displacement vector

$$\bar{d} = [\bar{\imath}_2 v + \bar{\imath}_3 w] = \begin{Bmatrix} v \\ w \end{Bmatrix} \tag{2.14}$$

is expanded in an infinite series of free vibration mode displacements

$$\bar{d} = \sum_{n=0}^{\infty} \sum_{i=1}^{2} \bar{\psi}_{n^i}(\theta)\eta_{n^i}(\tau) \tag{2.15}$$

in which the symmetric vector modes are

$$\bar{\psi}_{n^i} \equiv \begin{Bmatrix} (B/C)_{n^i} \sin n\theta \\ \cos n\theta \end{Bmatrix} \tag{2.16}$$

and the generalized coordinates $\eta_{n^i}(\tau)$ are calculated from

$$(\eta_{n^i})_{\tau\tau} + (\Omega_{n^i})^2\eta_{n^i} = \frac{1}{M_{n^i}} \int_0^{2\pi} \bar{q} \cdot \bar{\psi}_{n^i} a d\theta \tag{2.17}$$

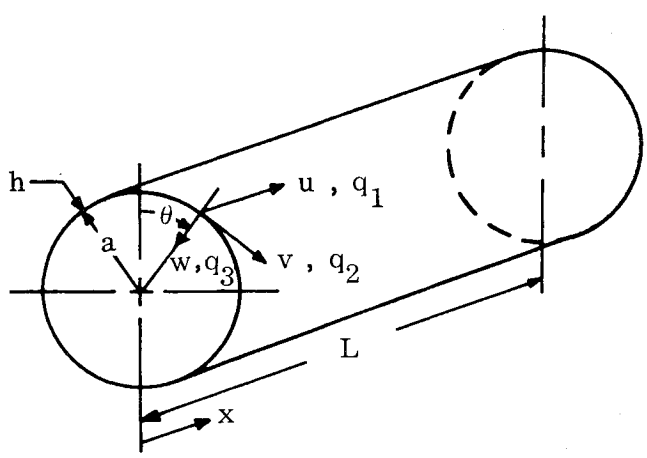

Fig. 1 Sign convention used for geometry, displacements, and loads of finite shell.

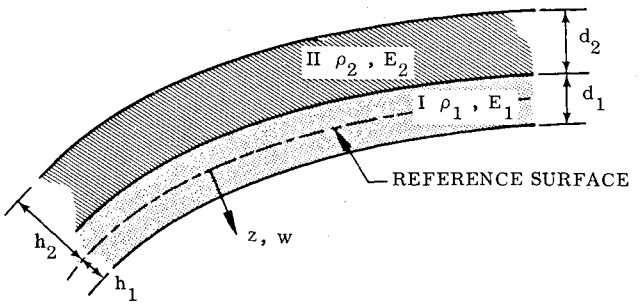

Fig. 2 Shell of two layers.

where

$$M_n{}^i \equiv \int_0^{2\pi} \bar{\psi}_n{}^i \cdot \bar{\psi}_n{}^i a d\theta \tag{2.18}$$

The angular frequency parameters $\Omega_n{}^i$ are the eigenvalues of the matrix

$$\begin{bmatrix} (\Omega^2 - n^2) & n \\ n & (\Omega^2 - 1 - k(n^2 - 1)^2) \end{bmatrix} \tag{2.19}$$

and the summation from one to two on the index i in Eq. (2.15) is necessary to account for the two eigenvalues $\Omega_n{}^i$ and eigenvectors $\bar{\psi}_n{}^i$ for each value of n.

Inspection of Eq. (2.19) reveals that, for $n = 0$ and $n = 1$, the roots $\Omega_0{}^1$ and $\Omega_1{}^1$ are zero. The root

$$\Omega_0{}^1 = 0 \tag{2.20}$$

corresponds to a rigid-body rotation; the root

$$\Omega_1{}^1 = 0 \tag{2.21}$$

corresponds to a rigid-body translation. These rigid-body motions arise when the length of the finite shell approaches infinity and the x boundary conditions are eliminated.

As a result of the assumptions that $q_1 = 0$ and that all variations in the x direction approach zero as the shell becomes infinitely long, the set of frequencies corresponding to the out-of-plane deflections of the cross sections has been eliminated from the analysis. This set corresponds roughly to the $\Omega_{mn}{}^2$ of the finite shell.

The natural frequencies and mode shapes for the vibrating infinite shell can be calculated in terms of n. The equation obtained by setting the determinant of the matrix of coefficients from Eq. (2.19) equal to zero is solved to give

$$\Omega_n{}^1 \approx k^{1/2}\{[n(n^2 - 1)]/[(n^2 + 1)^{1/2}]\} \tag{2.22}$$

and

$$\Omega_n{}^2 \approx (n^2 + 1)^{1/2} \tag{2.23}$$

The corresponding mode shape coefficients are

$$(B/C)_n{}^1 \approx 1/n \tag{2.24}$$

and

$$(B/C)_n{}^2 \approx -n \tag{2.25}$$

In the approximate equations, Eqs. (2.22) through (2.25), the quantity kn^2 has been neglected compared to unity. This procedure is valid; the circumferential wavelength should not be less than about ten times the shell thickness in a theory that neglects transverse shear and rotatory inertia.[10] Therefore,

$$n < 2\pi a/10h \tag{2.26}$$

hence

$$kn^2 < 0.03 \tag{2.27}$$

The values of the natural frequencies, as given in Eqs. (2.22) and (2.23), and the mode shapes given in Eqs. (2.24) and (2.25) agree with the values obtained by Baron and Bleich[3] for $L/a \to \infty$. In their report, these values occur for each n at the bottom of the columns labeled "lowest frequency" and "highest frequency." The values labeled "second lowest frequency" have been eliminated through the assumption that $u = 0$. Expressions (2.22–2.25) were found also by Rayleigh (Ref. 1, pp. 406, 417).

The stresses due to the displacement modes are

$$\sigma_\theta = \frac{E}{1 - \nu^2} \sum_{n=0}^{\infty} \sum_{i=1}^{2} D_n{}^i \cos n\theta \eta_n{}^i(\tau) \tag{2.28}$$

$$\sigma_x = \nu\sigma_\theta \tag{2.29}$$

$$\tau_{x\theta} = 0 \tag{2.30}$$

in which

$$D_n{}^i = [n(B/C)_n{}^i - 1 + (z/a)(n^2 - 1)] \tag{2.31}$$

Application to Shell of Two Layers

An equivalent boundary-value problem can be formulated for a thin shell composed of two bonded isotropic layers. Figure 2 shows a portion of such a shell. Both layers have the same Poisson's ratio. The densities and Young's moduli are different. The stress resultants are typically

$$N_x = \int_{-h_2}^{-d} \sigma_x{}^{II}\left(1 - \frac{z}{a}\right) dz + \int_{-d}^{h_1} \sigma_x{}^{I}\left(1 - \frac{z}{a}\right) dz \tag{2.32}$$

and

$$N_\theta = \int_{-h_2}^{-d} \sigma_\theta{}^{II} dz + \int_{-d}^{h_1} \sigma_\theta{}^{I} dz \tag{2.33}$$

where II refers to the outer layer and I to the inner layer. The stress-strain, strain-displacement, and equilibrium equations all have the same form as they did in the case of the homogeneous isotropic shell.

The quantity d is the distance from the reference surface to the material interface. This quantity may be determined such that the stress resultants have the same form as Flügge's.[9] If the terms involving $h_1{}^2$, $h_2{}^2$, and d^2 in Eqs. (2.32, 2.33, etc.) are set equal to zero, the following relation is obtained:

$$d = (E_1d_1{}^2 - E_2d_2{}^2)/[2(E_1d_1 + E_2d_2)] \tag{2.34}$$

The extensional rigidity D in Flügge's equations[9] becomes

$$D = (E_1d_1 + E_2d_2)/(1 - \nu^2) \tag{2.35}$$

and the flexural rigidity K becomes

$$K = \frac{1}{3}\frac{1}{1 - \nu^2}\left[E_1d_1{}^3 + E_2d_2{}^3 - \frac{3}{4}\frac{(E_1d_1{}^2 - E_2d_2{}^2)^2}{E_1d_1 + E_2d_2}\right] \tag{2.36}$$

The parameter k in Eqs. (2.1) through (2.3) is replaced by

$$k = K/Da^2 \tag{2.37}$$

All other considerations are the same as before, except that in calculating the stresses the reference surface is no longer the middle surface, but is located a distance d from the interface of the materials. Also, the new dimensionless time τ is given by

$$\tau = \omega_0{}^* t \tag{2.38}$$

3. Response of Two-Layered Shell to Radial Impulse Distributed Cosinusoidally Around Half of the Circumference and Uniformly along the Axis

The quantities $\eta_{mn}{}^i(\tau)$, the generalized coordinates defined by Eq. (2.9), depend upon the load $\bar{q}$. It will be assumed that the shell is initially at rest and that at $\tau = 0$ it is sub-

jected to a radial pressure distribution symmetric with respect to θ, applied as a square pulse of duration $\tau_0{}^*$. The dimensionless load $\bar{q}$ is taken as

$$\bar{q} = \bar{i}_3 q_0 \cos\theta \qquad -\pi/2 < \theta \leq \pi/2 \tag{3.1}$$

$$\bar{q} = 0 \qquad \pi/2 < \theta \leq 3\pi/2 \tag{3.2}$$

It can be shown that if $\Omega_{mn}{}^i\tau_0{}^* \ll 1$, the generalized coordinates $\eta_{mn}{}^i$ for the finite-length shell are

$$n \neq 1 \qquad \eta_{mn}{}^i = \frac{-2aLq_0{}^*\tau_0{}^*(1 - \cos m\pi)}{M_{mn}{}^i\Omega_{mn}{}^i m\pi} \times \left(\frac{\cos(n\pi/2)}{n^2 - 1}\right) \sin\Omega_{mn}{}^i\tau \tag{3.3}$$

$$n = 1 \qquad \eta_{m1}{}^i = \frac{2aLq_0{}^*\tau_0{}^*(1 - \cos m\pi)}{M_{m1}\Omega_{m1}{}^i m\pi}\left(\frac{\pi}{4}\right) \sin\Omega_{m1}{}^i\tau \tag{3.4}$$

The vector displacement $\bar{d}$ of the finite-length shell can now be computed from Eq. (2.7) and the stresses from Eqs. (2.11–2.13).

The load distribution given by Eqs. (3.1) and (3.2), applied to a shell of infinite length, leads to the generalized coordinates

$$\eta_n{}^i(\tau) = -2aq_0{}^*\tau_0{}^* \frac{1}{M_n{}^i\Omega_n{}^i} \frac{\cos(n\pi/2)}{(n^2 - 1)} \sin\Omega_n{}^i\tau \text{ for } n \neq 1 \qquad i \neq 1 \text{ when } n = 0 \tag{3.5}$$

and

$$\eta_1{}^i(\tau) = 2aq_0{}^*\tau_0{}^* \frac{1}{M_1{}^i\Omega_1{}^i}\frac{\pi}{4} \sin\Omega_1{}^i\tau \text{ for } n = 1 \qquad i \neq 1 \tag{3.6}$$

The requirements in Eqs. (3.5) and (3.6) that $i \neq 1$ omit the rigid-body modes for which $\Omega_n{}^i = 0$. These rigid-body motions are limiting cases that correspond to the pure torsion and the beam-type bending of a finite shell. From Eq. (2.15) with Eqs. (3.5) and (3.6), the dimensionless radial displacement w of the infinite-length shell can be obtained. It is given by

$$w = \frac{q_0{}^*\tau_0{}^*}{\pi}\left\{\sin\Omega_0{}^2\tau + \frac{\pi}{4(2)^{1/2}} \sin\Omega_1{}^2\tau \cos\theta - 2\sum_{n=2}^{\infty} \cos\frac{n\pi}{2} \frac{(n^2 + 1)^{1/2}}{(n^4 - 1)} \times \left[\frac{n}{(k)^{1/2}(n^2 - 1)} \sin\Omega_n{}^1\tau + \frac{1}{n^2 + 1} \sin\Omega_n{}^2\tau\right] \cos n\theta\right\} \tag{3.7}$$

The circumferential stress in the infinite shell can be computed by inserting the generalized coordinates given by Eqs. (3.5) and (3.6) into Eq. (2.28) to give

$$\sigma_\theta = \frac{-Eq_0{}^*\tau_0{}^*}{\pi(1 - \nu^2)}\left[\sin\Omega_0{}^2\tau + \frac{\pi}{2(2)^{1/2}} \sin\Omega_i{}^2\tau \cos\theta + 2\sum_{\substack{n=2 \\ n \text{ even}}}^{\infty} (-1)^{n/2} \frac{(n^2 + 1)^{1/2}}{(n^4 - 1)}\left(\frac{zn}{a(k)^{1/2}} \sin\Omega_n{}^1\tau - \sin\Omega_n{}^2\tau\right) \cos n\theta\right] \tag{3.8}$$

Table 1 Shell geometry and material properties

$d_1 = 0.06$ in.	$a = 6.0$ in.	$\rho_1 g = 0.065$ lb/in.^{3}
$d_2 = 0.20$ in.	$L = 18.0$ in.	$\rho_2 g = 0.044$ lb/in.^{3}
$E_1 = 6.5 \times 10^6$ psi	$\nu_1 = 0.3$	
$E_2 = 0.45 \times 10^6$ psi	$\nu_2 = 0.3$	

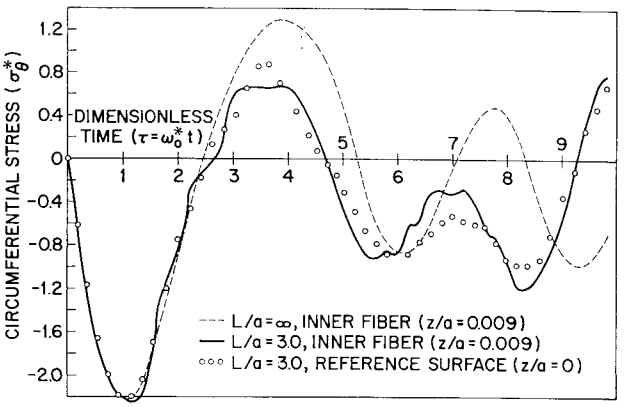

Fig. 3 Circumferential stress in two-layered shell for $\tau \leq 10$ at $x = L/2$, $\theta = 0$.

4. Numerical Results

Dimensionless displacements and stresses for the finite-length shell are evaluated from Eqs. (2.7 and 2.11–2.13), where m is summed from one to $M_{\max}$, and n is summed from zero to $N_{\max}$. A computer program written by Forsberg and Nagano[11] was used to calculate the frequencies and mode shapes. The geometry and material properties of the shell (see Fig. 2) are given in Table 1. These values when inserted into Eqs. (2.34, 2.36, and 2.37) yield $d = 5.63 \times 10^{-3}$ in., $K = 1.815 \times 10^3$ in.-lb, and $k = 9.55 \times 10^{-5}$, and one finds that

$$\omega_0{}^* = 2.11 \times 10^4 \text{ sec}^{-1} \qquad q_0{}^* = 11.4 \times 10^{-6}\, p_0$$

Hence, the dimensionless distance z/a from the reference surface to the inner fiber of the inner layer is about 0.009.

Convergence of the Series

When computing the response numerically, values must be assigned to $M_{\max}$ and $N_{\max}$, the upper limits of the truncated series expansions for the displacements and stresses. A thorough study of the convergence of the series expansions given by Eqs. (2.7 and 2.11–2.13) is made in Refs. 12 and 13. In Ref. 12 (Figs. 6.3–6.6), the rates of convergence with increasing $n(m = 1)$ for finite-length shells are found to approach those of infinite-length shells when $n > 10$. Figures 8.2–8.4 of Ref. 13 show the convergence of the coefficients in the series expansions for σ_x and σ_θ corresponding to $i = 1, 2, 3$, respectively. The "extensional" terms, which are those associated with $i = 2, 3$, the two higher frequencies for each set m, n, converge so rapidly that when $m > 9$, $n > 6$, and the next terms are less than 1% of the leading terms. The "flexural" terms ($i = 1$) converge approximately as $1/n^2$ when m is fixed and n is increased, but only as $\sin(m\pi x/L)/m$ (m odd and greater than about 20), when n is fixed, and m is increased. The assumption of uniform load ampli-

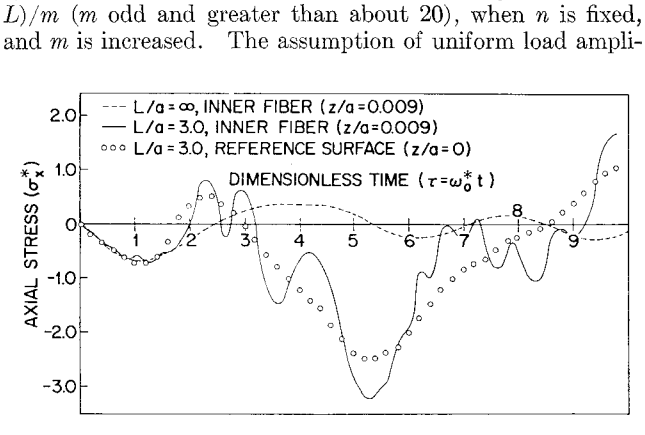

Fig. 4 Axial stress in two-layered shell for $\tau \leq 10$ at $x = L/2$, $\theta = 0$.

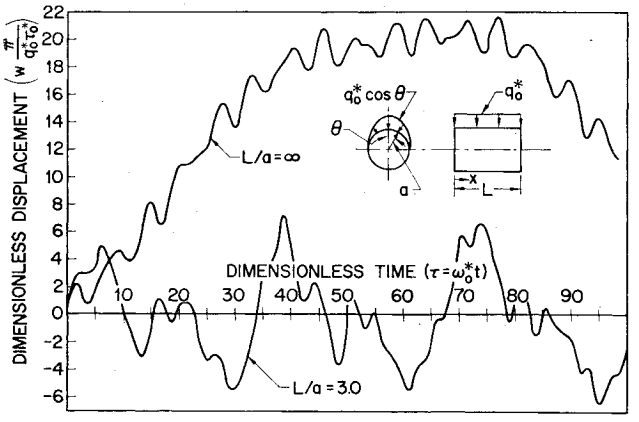

Fig. 5 Radial displacement of two-layered shell at $x = L/2$, $\theta = 0$.

tude along the axis is responsible for the slower convergence with n fixed and m increasing. The convergence of the series expansions for the displacements is at least as rapid as $1/n^3$ and $1/m^3$, for $i = 1, 2, 3$.

Upper limits of $M_{max} = 40$ and $N_{max} = 20$ were set in part by the above considerations. There is no doubt that all of the series expansions for displacement and stress have converged adequately for every value of m when n is greater than 20. The choice of an M_{max}, however, is influenced by the limitations of a shell theory that neglects transverse shear and rotatory inertia, as well as by the convergence considerations discussed above. Strictly speaking, if one uses a criterion that the half-wavelength should be greater than 10 times the thickness,[10] then the M_{max} for a shell whose geometry is given in Table 1 is about 10. The need to violate this limit for adequate convergence does not necessarily mean that the answer is wrong, but it should be checked by including the effects of transverse shear and rotatory inertia.

Numerical Calculations

For the finite-length shell, the time histories of σ_x^* and σ_θ^* at $x = L/2$, $\theta = 0$ at the inner fiber of the inner layer and at the reference surface, are presented in Figs. 3 and 4, where the normalized time range is $0 \leq \tau \leq 10$. For early times ($\tau < 2$) the dominant stress at $x = L/2$, $\theta = 0$ is circumferential compression. The maximum error in these results introduced by truncating the series at $m = 40$ is about ± 0.1, or 5% of the maximum value of σ_θ. This error is determined by considering the terms in the series expansions Eqs. (2.11) and (2.12) when m is large. For $m > 20$, the "extensional" ($i = 2, 3$) members are negligible and the "m" parts of the "flexural" ($i = 1$) terms have the form $\sin(m\pi x/L)/m$, m odd.[13] At $x = L/2$ this series is alternating, and hence the error in the partial sum is smaller than the absolute value of the next term ($m = 41$) in the series.

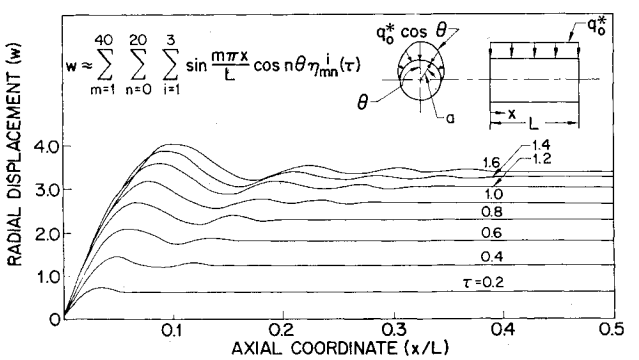

Fig. 6 Radial displacement of two-layered shell along the generator at $\theta = 0$ for $0.2 \leq \tau \leq 1.6$; $L/a = 3$.

Perhaps the most significant result evident in Figs. 3 and 4 is the magnitude of the axial stress σ_x generated in the laterally loaded cylindrical shell at $x = L/2$ and $\theta = 0$. Even though the boundary conditions [Eq. (2.5)] admit no axial constraint at the edges, the axial stress attains values that are greater than the maximum circumferential stress. It is probable that an important source of this stress is the longitudinal inertia of the vibrating shell.

The dimensionless radial displacement w, multiplied by $\pi/q_0^*\tau_0^*$ and evaluated at $x = L/2$, $\theta = 0$, is plotted in Fig. 5 for $0 \leq \tau \leq 80$. It is seen that the frequency bandwidth of the radial displacement is in a lower range than that of the stresses. Flexural modes, with which large displacements and low frequencies are associated, contribute little stress.

Also shown in Figs. 3–5 are the circumferential and axial stresses and radial displacement of a shell of infinite length. Points on these curves are found from Eqs. (3.7) and (3.8), where the upper limit on n is 20. The infinite-length solution agrees with the zero duration ($\tau_0^* = 0$) case of Ref. 7.

For very early times ($\tau < 2$) the infinite shell is a very good model of the shell of finite length ($L/a = 3$) as far as stress is concerned. For $\tau > 3$ however, the prediction of stress through the assumption of plane strain is poor, particularly in the case of axial stress.

Most of the radial displacement of the infinite-length shell occurs in the flexural component of the $n = 2$ mode. The amplitude is about four times as great as that predicted for the finite-length shell, and the dominant response frequency is about a seventh of that of the finite-length shell. Clearly the presence of the boundaries prevents large displacements and forces the shell to perform higher frequency extensional vibrations. The distributions of radial displacement and circumferential and axial stress along the generator $\theta = 0$ from $x = 0$ to $x = L/2$ are shown in Figs. 6 through 8. These distributions are plotted for various times in the early response ($\tau < 3$). The same range of m and n are used as before.

Figure 6 shows the dimensionless radial displacement w along the generator $\theta = 0$ for $0.2 \leq \tau \leq 1.6$ in steps of $\tau = 0.2$. For very early times most of the generator moves inward uniformly, the nonuniform motion being confined to a region near the edge. As time progresses, this edge "disturbance" propagates into the shell, so that by the time $\tau = 1.6$ most of the generator is "wavy." If $L = 18$ in., the velocity of this wave propagation is about 6.4×10^4 in./sec. The results are accurate since the convergence of the displacement series is faster than $1/m^3$, $1/n^3$.

Figure 7 depicts the dimensionless circumferential stress σ_θ^*, at $z/a = 0.009$ (inner fiber of inner layer) and $z/a = 0$, along the generator $\theta = 0$, for $0.2 \leq \tau \leq 3.0$. Again, the edge disturbance propagates into the shell. For $\tau \leq 0.6$,

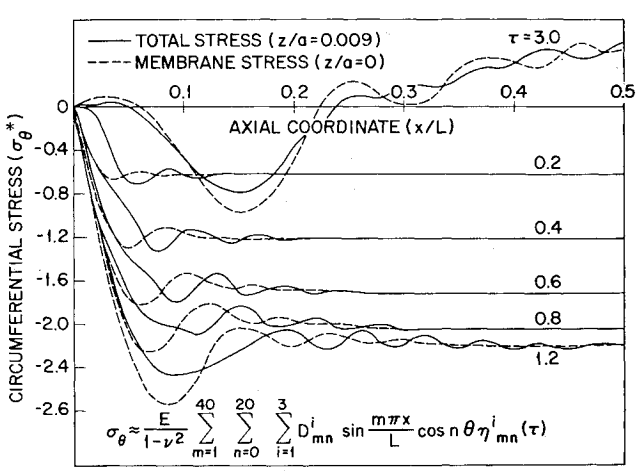

Fig. 7 Circumferential stress of two-layered shell along the generator at $\theta = 0$ for $0.2 \leq \tau \leq 3.0$; $L/a = 3$.

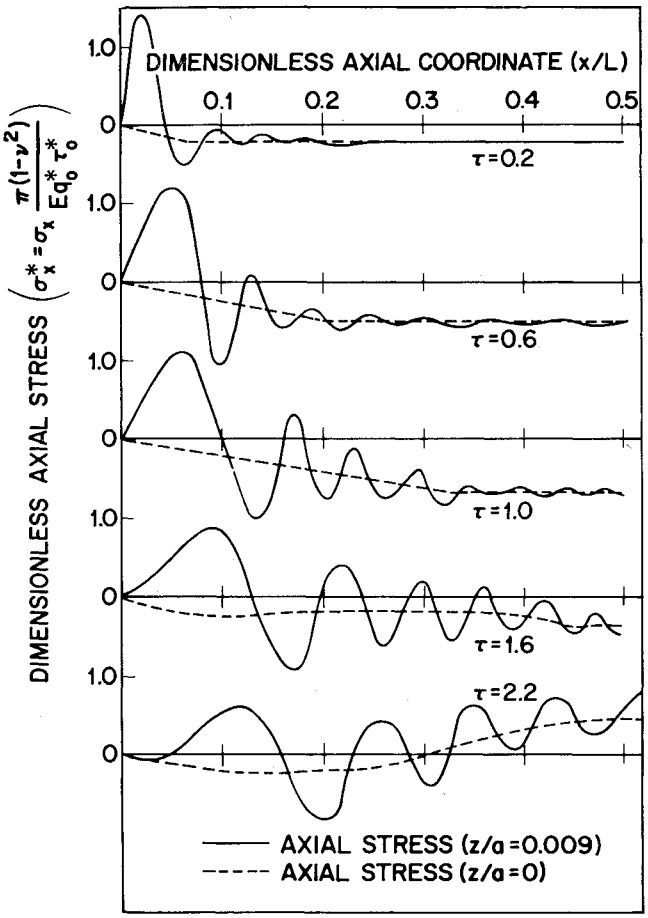

Fig. 8 Axial stress along the generator at $\theta = 0$ for $0.2 \leq \tau \leq 2.2$; $L/a = 3$.

the circumferential stress along most of the generator is uniform and compressive. As time progresses, the stress becomes nonuniform over the entire length of the shell. The maximum compressive stress occurs fairly near the edge.

The dotted lines show the membrane circumferential stress (σ_θ^* at $z/a = 0$). It is seen that the maximum membrane stress in the early time response is greater than the stress at the inner fiber, and that it exceeds the maximum stress at the center of the shell by about 30%. The maximum circumferential stress occurs at $x/L = 0.09$ at the outer fiber of the inner layer. The dimensionless time of its occurrence is $\tau = 1.4$.

In Fig. 8 the dimensionless axial stress at $z/a = 0.009$ and at $z/a = 0$ along the generator $\theta = 0$ is shown for the range $0.2 \leq \tau \leq 2.2$. Here the edge effect is indeed striking. High axial tension at the inner fiber, $z/a = 0.009$, develops very rapidly and very near the edge. When the geometry and material properties are given by Table 1, the strain rate corresponding to the maximum stress in the solid curve labeled $\tau = 0.2$ ($\sigma_0^* = 1.4$, $x/L = 0.02$) is about 400 in./(in. sec). This is the highest strain rate experienced anywhere in the shell for all time. It should be recalled that this high axial stress occurs near the edge even though the shell is completely free to move in the axial direction at $x = 0$ and $x = L$. Any boundary conditions that would restrain the edges either structurally or inertially would probably increase the maximum axial stress encountered.

Again, the solid lines represent stress at the inner fiber ($z/a = 0.009$), and the dotted lines represent the stress at the reference surface ($z/a = 0$). It is seen in Fig. 8 that, near the edge, the axial stress varies considerably through the thickness, and that for $x/L \geq 0.2$ the stress is almost constant through the thickness.

The propagation velocity of the axial membrane stress edge disturbance can be closely approximated by noticing in Fig. 8 that, for $\tau \leq 1.0$, the plots of axial membrane stress vs distance along the generator consist of two straight lines with sharp discontinuities in slope. For a shell of two layers with the geometry and material properties summarized in Table 1, the velocity of this slope discontinuity is about 128,000 in./sec. A calculation of the "effective" speed of sound in the composite wall from the formula

$$c^2_{\text{eff}} = (E_1 d_1 + E_2 d_2)/(\rho_1 d_1 + \rho_2 d_2) \qquad (4.1)$$

yields $c_{\text{eff}} = 121{,}000$. It is clear that this edge disturbance is transmitted at about the "effective" speed of sound in the shell wall.

The accuracy of the solid curves in Figs. 6 through 8 was tested by setting the upper limit on m equal to 80 instead of 40. The results, presented in Ref. 14, show that the radial displacement (Fig. 6) is virtually unaffected, that the peak circumferential stress ($\tau = 1.2$, Fig. 7) is unchanged, and that the peak axial stress is about 5% lower and occurs at a slightly earlier time than that shown in Fig. 8 ($\tau = 0.2$). The membrane stresses ($z/a = 0$) are unchanged.

References

[1] Lord Rayleigh, Strutt, J. W., and Baron, M. L., *Theory of Sound* (Dover Publications, Inc., New York, 1945), 2nd ed.

[2] Arnold, R. N. and Warburton, G. B., "Flexural vibrations of the walls of thin cylindrical shells having freely supported ends," Proc. Roy. Soc. (London) **A197**, 238–256 (1949).

[3] Baron, M. L. and Bleich, H. H., "Tables for frequencies and modes of free vibration of infinitely long thin cylindrical shells," J. App. Mech. **21**, 179–184 (1954).

[4] Yu, Y-Y., "Free vibrations of thin cylindrical shells having finite lengths with freely supported and clamped edges," J. Appl. Mech. **22**, 547–552 (1954).

[5] Yu, Y-Y., "Vibrations of thin cylindrical shells analyzed by means of Donnell-type equations," J. Aerospace Sci. **25**, 699–715 (1958).

[6] Forsberg, K., "Influence of boundary conditions on the modal characteristics of thin cylindrical shells," AIAA J. **2**, 2150–2157 (1964).

[7] Humphreys, J. F. and Winter, R., "Dynamic response of a cylinder to a side pressure pulse," AIAA J. **3**, 27–32 (1965).

[8] Sheng, J., "The response of a thin cylindrical shell to transient surface loading," AIAA J. **3**, 701–709 (1965).

[9] Flügge, W., *Stresses in Shells* (Springer-Verlag, Berlin, 1960), Chap. 5, pp. 219, 212.

[10] Goodier, J. N. and McIvor, I. K., "Dynamic stability and non-linear oscillations of cylindrical shells," Stanford Univ. T R 132, Chap. II (June 1962).

[11] Forsberg, K. and Nagano, N., "Vibration characteristics—thin circular cylinders and associated computer program," Lockheed Missiles and Space Co. Rept. 3-71-63-3 (June 1963).

[12] Bushnell, D., "Dynamic response of circular cylindrical shells to time-dependent loads—Part I," Lockheed Missiles and Space Co., LMSC-804538 (November 1964).

[13] Bushnell, D., "Dynamic response of circular cylindrical shells to time-dependent loads—Part II," Lockheed Missiles and Space Co., LMSC-A708254 (November 1964).

[14] Bushnell, D., "Dynamic response of circular cylindrical shells to time-dependent loads—Part III," Lockheed Missiles and Space Co., LMSC-804731 (November 1964).